Received: 22 February 2024 | Revised: 24 April 2024 | Accepted: 30 April 2024

DOI: 10.1002/agt2.588

Aggregate WILEY

RESEARCH ARTICLE

Linker aggregation engineering of TADF materials to tune carrier balance for highly efficient organic LEDs with long operational lifetime

Zhen Zhang[1] | **Rongrong Xia**[1] | **Ke Wang**[1] | **Youjun Wu**[1] | **Panpan Zang**[1] | **Xuemin Gan**[2] | **Zhangcheng Liao**[1] | **Bin Wei**[1] | **Peng Wu**[1] | **Stefan Bräse**[2,3] | **Zixing Wang**[1]

[1]Key Laboratory of Advanced Display and System Applications, Ministry of Education, Shanghai University, Shanghai, China

[2]Institute of Organic Chemistry, Karlsruhe Institute of Technology (KIT), Karlsruhe, Germany

[3]Institute of Biological and Chemical Systems-Functional Molecular Systems (IBCS-FMS), Karlsruhe Institute of Technology (KIT), Karlsruhe, Germany

Correspondence
Peng Wu and Zixing Wang, Key Laboratory of Advanced Display and System Applications, Ministry of Education, Shanghai University, Yanchang 149, 200072 Shanghai, China.
Email: jjwupeng@shu.edu.cn; zxwang78@shu.edu.cn

Stefan Bräse, Institute of Organic Chemistry, Karlsruhe Institute of Technology (KIT), Kaiserstrasse 12, 76131 Karlsruhe, Germany.
Email: braese@kit.edu

Funding information
National Key R&D Program of China, Grant/Award Number: 2022YFE0109000; National Natural Science Foundation of China, Grant/Award Number: 21975152; China Postdoctoral Science Foundation, Grant/Award Number: 2022M722028; Deutsche Forschungsgemeinschaft, Grant/Award Number: 3DMM2O–EXC–2082/1–390761711

Abstract

Thermally activated delayed fluorescence (TADF) molecules are regarded as promising materials for realizing high-performance organic light-emitting diodes (OLEDs). The connecting groups between donor (D) and acceptor (A) units in D–A type TADF molecules could affect the charge transfer and luminescence performance of TADF materials in aggregated states. In this work, we design and synthesize four TADF molecules using planar and twisted linkers to connect the aza-azulene donor (D) and triazine acceptor (A). Compared with planar linkers, the twisted ones (**Az-NP-T** and **Az-NN-T**) can enhance A–A aggregation interaction between adjacent molecules to balance hole and electron density. As a result, highly efficient and stable deep-red top-emission OLEDs with a high electroluminescence efficiency of 57.3% and an impressive long operational lifetime (LT_{95} ~ 30,000 h, initial luminance of 1000 cd m^{-2}) are obtained. This study provides a new strategy for designing more efficient and stable electroluminescent devices through linker aggregation engineering in donor–acceptor molecules.

KEYWORDS

acceptor stacking, balanced carrier transfer, host materials, long device lifetime, thermally activated delayed fluorescence

1 | INTRODUCTION

Thermally activated delayed fluorescence (TADF) molecules with pure organic components are comparable to phosphorescent materials in internal quantum efficiency, which are considered as the third-generation organic light-emitting diode (OLED) materials.[1] Especially, a small energy gap difference (ΔE_{ST}) between the lowest triplet state (T_1) and lowest singlet state (S_1) is conducive to achieving fast reverse intersystem crossing (RISC) and short exciton lifetime in TADF molecules.[2] One of the promising design strategies for TADF with small ΔE_{ST} is to develop twisted donor–acceptor (D–A) molecules.[3] However, a small ΔE_{ST} of TADF materials would reduce the radiative decay rate for the donor–acceptor.[4] As a result, the exciton quenching at high concentrations easily happened for the TADF molecules as emitters.[5–7] When used in the devices, it easily leads to serious roll-off and short operational lifetime, especially at high voltage and brightness.[8]

The host–guest system effectively reduces the quenching effect by dispersing the emitter in the host matrix.[9] The ideal host materials should have efficient energy transfer to

Zhen Zhang and Rongrong Xia contributed equally to this work.

guests, good thermal stability, and balanced carrier transfer ability.[10] TADF materials containing donor and acceptor frameworks are excellent host candidates with bipolar properties. Highly efficient and stable devices based on TADF hosts with phosphorescent guests have been reported.[11] For most bipolar host materials, carbazole and its derivatives are often selected as hole donors due to their rigid structure, high triplet energy, and good hole transport properties. Due to the excellent electron mobility, the 1,3,5-triazine derivatives have been used as electron acceptors for host materials.[12] Particularly, connecting donor and acceptor with an ortho-substitution type using a π-conjugation linking bridge is a very effective strategy to construct TADF host materials because ortho-linking can provide both forms of charge transfer through bond and space, thereby effectively avoiding exciton concentration quenching.[13] However, in the aggregated state, the spatial packing of molecules can greatly affect their TADF properties, such as RISC. In addition, the packing morphology in the aggregated state is closely related to their chemical groups, as these molecules are often driven to aggregate by CH–π interactions.[14] Therefore, it is important to regulate the aggregation behavior through chemical design to optimize the performance of TADF molecules. This requires a deep understanding of the interactions between molecules and the structure of the aggregated state, in order to rationally design molecular structures, optimize the stacking method, and ultimately improve the performance of OLEDs.[15] One possible strategy is to introduce specific distorted structures into the connecting groups. Distorted structures can also suppress harmful aggregation phenomena (such as π–π stacking) through spatial repulsion effects, thereby optimizing the performance of TADF molecules.

In this study, four ortho-substituted molecules containing aza-azulene donor and 4,6-diphenyl-1,3,5-triazine acceptor connected by two planar linkers (phenanthrene and triphenylene) and two twisted linkers (1-phenylnaphthalene and 1,1′-binaphthalene) were designed and synthesized. These molecules, **Az-P-T**, **Az-TP-T**, **Az-NP-T**, and **Az-NN-T**, show TADF features and fast RISC processes due to twisted resonance of aza-azulene unit. **Az-NP-T** and **Az-NN-T** especially demonstrate enhanced and balanced carrier transport properties induced by acceptor aggregation interactions. Using these molecules as hosts, highly efficient and stable deep-red OLEDs with an external quantum efficiency (EQE) of 57.3% and an impressive long device lifetime LT_{95} ~ 30,000 h (Initial luminance of 1000 cd m^{-2}) are obtained.

2 | RESULT AND DISCUSSION

2.1 | Synthesis, thermal, and electrochemical properties

Four molecules were prepared with 65%–72% yields via a nucleophilic substitution reaction under basic conditions (Scheme 1 and details in Supporting Information). The chemical structure of **Az-P-T**, **Az-TP-T**, **Az-NP-T**, and **Az-NN-T** was thoroughly characterized by $^{1}H/^{13}C$ NMR and high-resolution mass analyses (HRMS).

The thermal properties of these four molecules were investigated by thermogravimetric analysis (TGA) under nitrogen atmosphere, and the results are presented in Figure S1. All these four molecules, **Az-P-T**, **Az-TP-T**, **Az-NP-T**, and **Az-NN-T**, possess high thermal stability with decomposition temperatures (T_d, at 5% weight loss) of 452, 472, 445, and 462°C, respectively. It indicated that these materials would perform well in preparing the device by evaporation strategy.

The electrochemical properties were carried out by cyclic voltammetry (CV) and differential pulse voltammetry (DPV) to estimate their HOMOs. Figure S2 shows that these molecules show similar quasi-reversible oxidation potentials due to the same donor fragment, which can easily oxidize. From the onset of oxidation waves, the HOMO energy levels were calculated to be −5.85, −5.89, −5.88, and −6.00 eV for **Az-P-T**, **Az-TP-T**, **Az-NP-T**, and **Az-NN-T**, respectively. The LUMO energy levels could be calculated by the difference between HOMO and band gap (*Eg*), which were −2.83, −2.88, −2.86, and −2.99 eV for **Az-P-T**, **Az-TP-T**, **Az-NP-T**, and **Az-NN-T**, respectively.

2.2 | Theoretical calculation and analysis

Density functional theory (DFT) and time-dependent DFT (TD-DFT) calculations were performed to understand the electronic and structural properties further. The molecule-optimized configuration was carried out using GB3LYP/6–31G (d, p) and GB3LYP/Def2-TZVP basis set to estimate the excited state energies by the Beijing density function (BDF).[16] The Multiwfn program was used to visualize the distributions and natural transition orbital (NTO).[17] As shown in Figure 1, due to the large rigid and steric hindrance, the optimized geometries of four molecules with twisted molecular geometry are beneficial for separating frontier molecular orbital (FMO). The HOMOs were mainly located on aza-azulene donors, and the LUMOs were dispersed on triazine acceptors with partly spreading to linker units. The spatial distance between the sp^3-N of aza-azulene donor and sp^2-N of triazine planes are 2.770, 2.730, 2.767, and 2.766 Å for **Az-P-T**, **Az-TP-T**, **Az-NP-T**, and **Az-NN-T**, respectively (Figure 1). The short distance can trigger the lone pair…π interaction and facilitate the intramolecular charge transport.[18] The singlet/triplet energy levels of **Az-P-T**, **Az-TP-T**, **Az-NP-T**, and **Az-NN-T** were 2.49/2.29, 2.45/2.30, 2.46/2.29, and 2.45/2.29 eV with the calculated ΔE_{ST} of 0.20, 0.15, 0.17, and 0.16 eV, respectively. The NTO method was used to analyze transition characteristics (Figure 1 and Figures S3–S6). The S_1 states of all these four compounds show the CT character between the aza-azulene donor and the triazine acceptor. For excited T_1 states, it can be seen that their hole distributions are similar, mainly on the aza-azulene unit, while the electron distributions are different. In **Az-P-T** and **Az-TP-T**, the electrons of excited T_1 are mainly located at the middle linking groups. This means that the T_1 exciton of these two compounds preferentially forms the delocalization of the electron cloud between aza-azulene and the linker rather than form the charge transfer state between aza-azulene and the triazine group. However, for **Az-NP-T** and **Az-NN-T**, their electrons of excited T_1 are still mainly distributed on the aza-azulene donor, which makes their T_1 possess obvious LE characteristics. The LE features of excited triplet states were mixed in T_2 of **Az-P-T** and T_3 of **Az-TP-T**. As reported by Kaji and Ren, ^{3}LE state is a key point to achieve fast RISC.[19] The difference between ^{1}CT and ^{3}LE of **Az-P-T**,

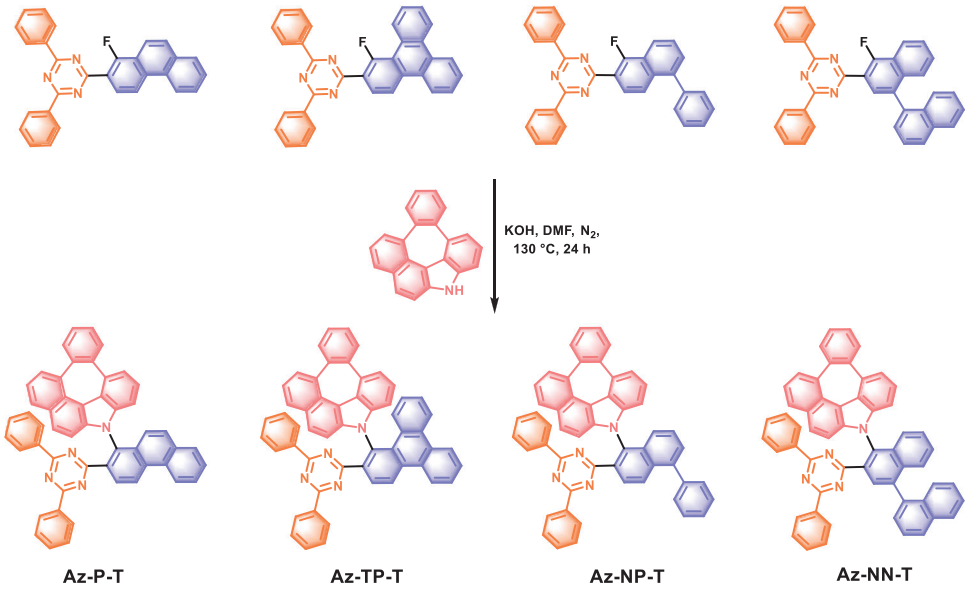

SCHEME 1 Synthetic routes for **Az-P-T**, **Az-TP-T**, **Az-NP-T**, and **Az-NN-T**.

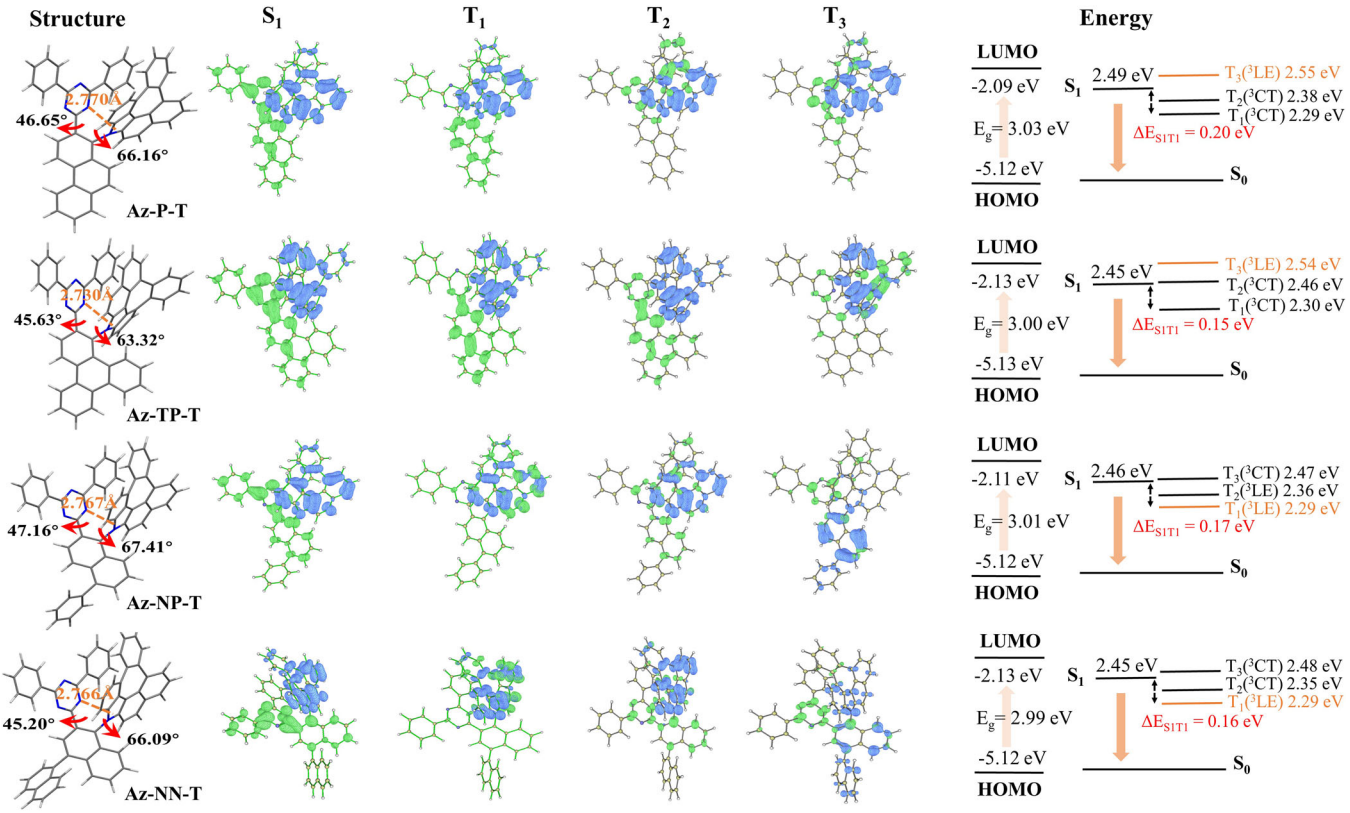

FIGURE 1 The optimized molecular structures, natural transition orbital analysis of the S_1 and T_1 (blue and green represent the hole and electron, respectively), and energy levels for **Az-P-T**, **Az-TP-T**, **Az-NP-T**, and **Az-NN-T**.

Az-TP-T, **Az-NP-T**, and **Az-NN-T** were 0.06, 0.09, 0.17, and 0.16 eV. It can be seen that **Az-P-T** and **Az-TP-T** possess smaller differences than that of **Az-NP-T** and **Az-NN-T**, which is helpful to achieve fast RISC process.

2.3 | Photophysical properties

The ultraviolet–visible (UV–vis) absorption of these four molecules in a dilute 2-methyltetrahydrofuran (2-Me-THF) solution was measured, and the results are shown in Figure 2. **Az-P-T**, **Az-TP-T**, **Az-NP-T**, and **Az-NN-T** exhibited the high-intensity π–π^* absorption at below 300 nm, weak n–π^* absorption at the 320–360 nm, and broad intramolecular CT transition absorption above 360 nm. The *E*g estimated from the absorption edge is 3.02, 3.01, 3.02, and 3.01 eV for **Az-P-T**, **Az-TP-T**, **Az-NP-T**, and **Az-NN-T**, respectively. The effect of solvent polarity was studied to verify charge transfer emission (Figure 2). In cyclohexane, the photoluminescence (PL) peaks of these molecules indicate the

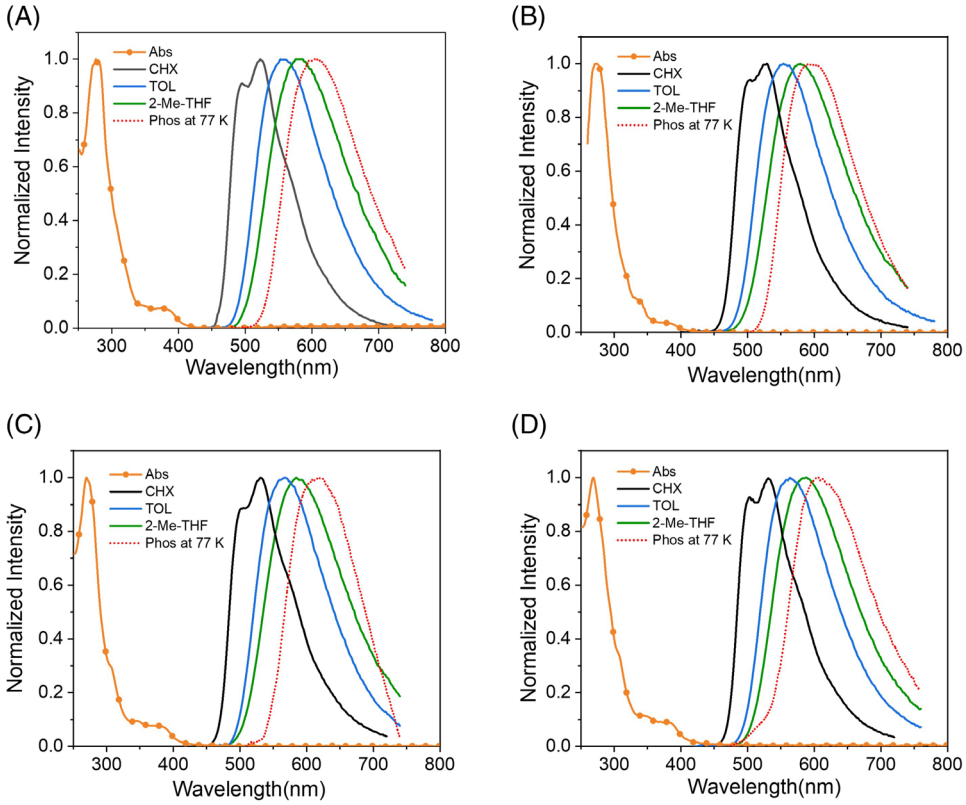

FIGURE 2 Ultraviolet–visible absorption spectra in 2-methyltetrahydrofuran (2-Me-THF), fluorescence spectra in different solvents, and phosphorescence (Phos) spectra at 77 K in 2-Me-THF for (A) **Az-P-T**, (B) **Az-TP-T**, (C) **Az-NP-T**, and (D) **Az-NN-T**.

mixture emission of singlet charge transfer (^{1}CT) from the D–A and locally excited (^1LE_D) from the donor state transition. With the increasing polarity of solvents, the emission peaks of **Az-P-T**, **Az-TP-T**, **Az-NP-T**, and **Az-NN-T** red-shift show broad and featureless emission profiles, indicating the typical CT state emission. The phosphorescence spectra at 77 K of the four molecules in 2-Me-THF were also measured (Figure 2). According to the onsets of the fluorescence and phosphorescence spectra of **Az-P-T**, **Az-TP-T**, **Az-NP-T**, and **Az-NN-T**, the S_1 and T_1 states were estimated at 2.46/2.34, 2.48/2.35, 2.45/2.28, and 2.44/2.31 eV, respectively. The corresponding ΔE_{ST} were 0.12, 0.13, 0.17, and 0.13 eV, which align with the theoretical calculation values. The small ΔE_{ST} can promote the RISC process, indicating the potential TADF property for **Az-P-T**, **Az-TP-T**, **Az-NP-T**, and **Az-NN-T**.

To further prove the TADF characteristic of these four molecules, the neat and doped films into poly-(methyl methacrylate) (PMMA) with various concentrations were prepared. At a low doping concentration of 1% in PMMA films, the emission peaks of **Az-P-T**, **Az-TP-T**, **Az-NP-T**, and **Az-NN-T** are 516, 509, 525, and 522 nm, respectively (Figure S7), which is similar to intramolecular CT emission in cyclohexane solution. This is because, at low doping concentrations, the matrix limits intermolecular interactions to ensure the intramolecular CT emission from the single molecule. As the concentration increases, the emission peak red-shifted because of the solid solvation effect or intermolecular CT,[20] and the results are summarized in Table S1. The PL emission peaks in neat films of **Az-P-T**, **Az-TP-T**, **Az-NP-T**, and **Az-NN-T** are 552, 547, 559, and 554 nm, respectively.

The transient PL decays of these molecules in neat films were measured under nitrogen atmosphere (Figure 3 and Table 1). The PL decay curve of all films exhibits biexponential decays, including prompt component (τ_p) and delayed component (τ_d). The τ_p of **Az-P-T**, **Az-TP-T**, **Az-NP-T**, and **Az-NN-T** were estimated to be 10.5, 14.7, 7.9, and 7.8 ns, and the τ_d were 5.8, 7.5, 6.7, and 6.7 μs, respectively. These molecules' kinetic parameters and rate constants were calculated and obtained (Table S2).[21] The RISC rate constants (k_{RISC}) of neat films for **Az-P-T**, **Az-TP-T**, **Az-NP-T**, and **Az-NN-T** are 6.6×10^5, 4.6×10^5, 4.0×10^5, and 4.5×10^5 s^{-1}, respectively. The large k_{RISC} of four molecules is attributed to the efficient charge transfer through bond charge transfer (TBCT) and space charge transfer emission (TSCT) due to their ortho-twisted molecular configurations and short spatial distance between aza-azulene donor and triazine planes, as reported in the literature.[22–24]

2.4 | Electroluminescence

Given that **Az-P-T**, **Az-TP-T**, **Az-NP-T**, and **Az-NN-T** possess good thermal stabilities, TADF characteristics, fast RISC processes, and high T_1 states, they are very suitable to be used as host materials for red phosphorescent emitter to fabricate OLED devices. The single-carrier devices were fabricated to gain insight into the carrier transport capabilities of these four host molecules. The hole-only device structures: ITO/HTL022: PD001 (3%, 10 nm)/HTL022 (40 nm)/host (36 nm)/HTL022 (10 nm)/Al (80 nm), and the electron-only devices structures: ITO/ASFT (10 nm)/host (36 nm)/ASFT:Liq (1:1, 30 nm)/Liq (1 nm)/Al

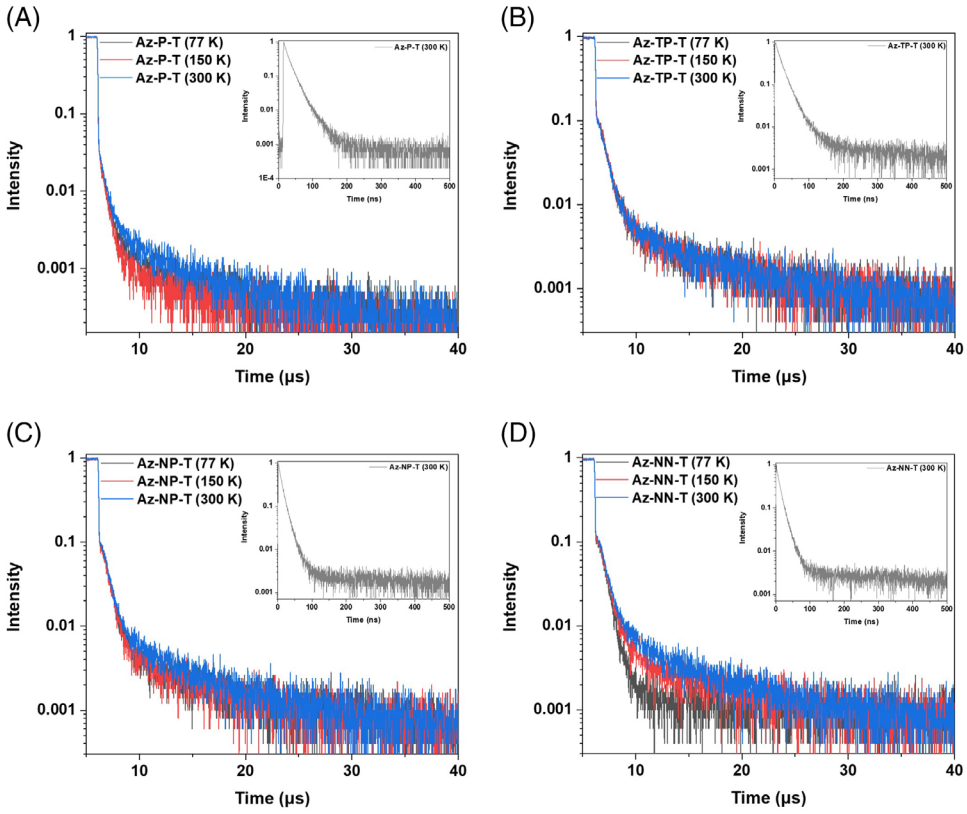

FIGURE 3 The temperature-dependent transient photoluminescence (PL) decay spectra for (A) **Az-P-T**, (B) **Az-TP-T**, (C) **Az-NP-T**, and (D) **Az-NN-T** (insert: transient PL decay spectra in the range of 0–500 ns at room temperature).

TABLE 1 Photophysical properties for **Az-P-T**, **Az-TP-T**, **Az-NP-T**, and **Az-NN-T**.

	λ_{PL}[a] [nm]	HOMO [eV]	LUMO [eV]	E_g[b] [eV]	S_1[c] [eV]	T_1[d] [eV]	ΔE_{ST}[e] [eV]	τ_p[f] [ns]	τ_d[g] [μs]	k_{ISC}[h] [$\times 10^7$ s^{-1}]	k_{RISC}[i] [$\times 10^5$ s^{-1}]
Az-P-T	495,523/553/606/581	−5.85	−2.83	3.02	2.46	2.34	0.12	10.5	5.8	7.1	6.6
Az-TP-T	498,529/554/579/596	−5.89	−2.88	3.01	2.48	2.35	0.13	14.7	7.5	4.8	4.6
Az-NP-T	498,531/568/584/616	−5.88	−2.86	3.02	2.45	2.28	0.17	7.9	6.7	8.0	4.0
Az-NN-T	500,531/564/588/614	−6.00	−2.99	3.01	2.44	2.31	0.13	7.8	6.7	8.6	4.5

[a]The PL spectra in cyclohexane/toluene/2-methyltetrahydrofuran/dichloromethane solution.
[b]Estimated from the absorption edge in 2-Me-THF.
[c]Calculated from the steady-state emission spectra.
[d]Estimated from the phosphorescence spectra at 77 K.
[e]Energy gap between S_1 and T_1 states.
[f]Lifetime of prompt fluorescence under nitrogen atmosphere.
[g]Lifetime of delayed fluorescence under nitrogen atmosphere.
[h]Intersystem crossing rate.
[i]Reverse intersystem crossing rate.

(80 nm), N-[1,1′-diphenyl]−4-yl-9,9-di-methyl-N-[4-(9-phenyl-9H-carbazol-3-yl)phenyl]−9H-fluoren-2-amine (HT-L022), α,α'-[3-[cyano(3-cyano-2,4,5-trifluoro-6-methylphenyl)methylene]−1,2-cyclopropanediylidene]bis[4-cyano-2,3,5,6-tetrafluo-robenzeneacetonitrile] (PD001), 4-(3-(4,6-diphenyl-1,3,5-triazin-2-yl)phenyl)spiro[fluorene-9,5′-indeno[1,2-*c*]pyridine] (ASFT, Figure S9). The hosts are **Az-P-T**, **Az-TP-T**, **Az-NP-T**, and **Az-NN-T**, respectively. The current density–voltage curves are shown in Figure 4. For **Az-P-T** and **Az-TP-T** containing phenanthrene and triphenylene as linking groups, their hole transport capacities are much higher than their electron transport capacities, especially at high voltages. Unbalanced carrier transport can easily cause exciton quenching, leading to serious device roll-off and poor stability. However, **Az-NP-T** and **Az-NN-T** containing 1-phenylnaphthalene and 1,1′-binaphthalene as linking groups exhibit balanced hole and electron transport capabilities at both high and low voltages. This is very helpful for obtaining low-efficiency roll-off and good device stability at high brightness.

To explain why there is such a big difference in the carrier transport capabilities of these four molecules, we performed molecular simulation calculations. We found that in their molecular packing, the triazine acceptor groups have better overlap and packing for **Az-NP-T** and **Az-NN-T**. The two triazine units have a larger overlapping area and a closer distance, and the distance between the nearest nitrogen atoms is only 3.544 Å for **Az-NP-T** and 3.423 Å for **Az-NN-T**

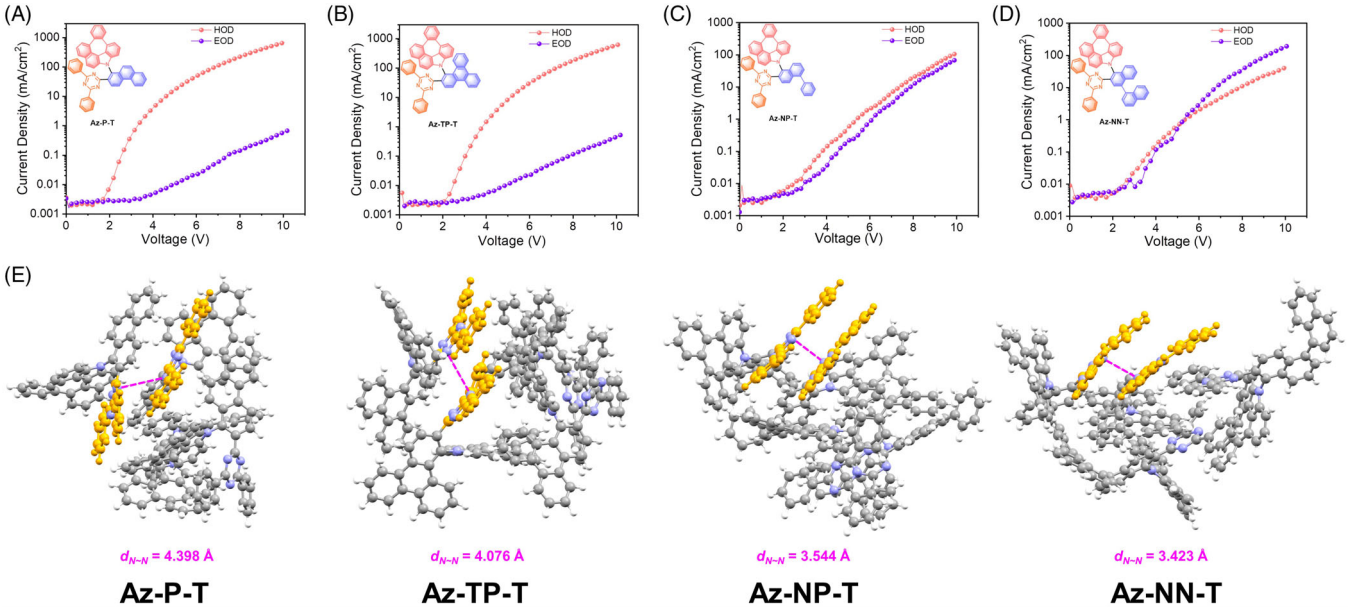

FIGURE 4 Current density–voltage characteristics of the electron-only and hole-only devices for (A) **Az-P-T**, (B) **Az-TP-T**, (C) **Az-NP-T**, and (D) **Az-NN-T** as host, respectively. (E) Molecular packing and distance of two nearest nitrogen atoms between two triazine units.

(Figure 4). But there is no obvious triazine overlap for **Az-P-T** and **Az-TP-T**, and the distance between its nearest nitrogen atoms is above 4.398 Å for them (4.398 Å for **Az-P-T** and 4.076 Å for **Az-TP-T**). The different molecular packing patterns of these molecules could be ascribed to the different connecting bridges utilized in them. Compared with the planar connecting bridges, phenanthrene (in **Az-P-T**), and triphenylene (in **Az-TP-T**), the substituted naphthalene linkers used in **Az-NP-T** and **Az-NN-T** have a twisted structure. As a result, the linking bridges in **Az-NP-T** and **Az-NN-T** cannot stack well with the planar triazine unit of another molecule, while this can promote the formation of better π-stacking between its triazine group and the adjacent triazine group, which applies an additional channel for electron transport. Therefore, the enhanced electron transport ability of **Az-NP-T** and **Az-NN-T** could be attributed to their better acceptor space interactions. Furthermore, for ortho-linked donor–acceptor molecules, the molecular packing form can be tuned by changing the linking bridge, and ultimately, the carrier transport ability can be adjusted.

To investigate the electroluminescence properties of **Az-P-T**, **Az-TP-T**, **Az-NP-T**, and **Az-NN-T**, PhOLEDs with RD-1 as emitters were fabricated. The bottom-emitting red PhOLED device is: indium tin oxide (ITO)/HTL022: PD001 (2%, 10 nm)/HTL022 (40 nm)/host: RD-1 (2%, 20 nm)/ASFT (10 nm)/ASFT:Liq (1:1, 30 nm)/Liq (1 nm)/Al (80 nm), (3,7-diethyl-4,6-nonanedionato-κO_4,κO_6)bis[2,4-dimethyl-6-[6-(1-methyle-thyl)−1-isoquinolinyl-κN]phenyl-κC]iridium (RD-1), and the results as shown in Table S4 and Figure S8. The devices based on **Az-NP-T**, and **Az-NN-T** exhibited current efficiency (CE) over 28 cd A^{-1} and EQE of 29%, which are better than those of devices based on **Az-P-T** and **Az-TP-T** (CE around 24 cd A^{-1} and EQE of 25%). More importantly, since top-emitting structure is a common strategy in commercial OLED devices, the top-emitting devices are fabricated and structured as: ITO/HTL022: PD001 (2%, 10 nm)/HTL022 (130 nm)/HTL001 (90 nm)/EBL001 (10 nm)/host: RD-1 (2%, 40 nm)/ASFT: Liq (1:1, 35 nm)/Yb (1 nm)/Ag (14 nm)/CPL (top capping layer, HTL001, 70 nm), *N*-([1,1′-biphenyl]−2-yl)-*N*-(9,9-dimethyl-9*H*-fluoren-2-yl)−9,9′-spirobi[fluoren]−2-amine (HTL001), *N*-([1,1′-biphenyl]−2-yl)-*N*- (9,9-dimethyl-9H-fluoren-2-yl) −9,9-diphenyl-9H-fluoren-2-amine (EBL001). The **Az-P-T**, **Az-TP-T**, **Az-NP-T**, and **Az-NN-T** are host materials for devices A, B, C, and D, respectively. As shown in Table 2 and Figure S9, under different current densities, the maximum emission wavelength of four devices is consistent with the emission peak of red guest material, RD-1. No emission peak from the host material and other functional layer materials is detected. These results demonstrated that the host materials of **Az-P-T**, **Az-TP-T**, **Az-NP-T**, and **Az-NN-T** could transfer energy to the guest dopant. The deep-red emission peak is 626–628 nm with color coordinates of (0.69, 0.31). The turn-on voltages of devices A, B, C, and D were 2.9, 3.4, 2.7, and 2.8 V, respectively. The current density–voltage–luminance (*J*–*V*–*L*) of devices A, B, C, and D are shown in Figure 5C. The maximum luminance of devices A, B, C, and D is 25570, 25790, 25320, and 26270 cd m^{-2}, respectively. The maximum CE (CE_{max}) of devices A, B, C, and D is 62.1, 57.4, 62.5, and 61.2 cd A^{-1}, and the maximum power efficiency (PE_{max}) is 60.7, 50.8, 65.6, and 64.6 lm W^{-1} (Figure 5D,E and Table 2), respectively. For **Az-P-T** and **Az-TP-T**, the devices A and B show the EQE_{max} of 54.2% and 46.2%, respectively. For **Az-NP-T** and **Az-NN-T**, the devices C and D with **Az-NP-T** and **Az-NN-T** as hosts show higher EQE_{max} of 57.3% and 55.0%, respectively. At high luminescence of 10,000 cd m^{-2}, the EQE of devices C and D can still be maintained above 50% (50.7% for device C and 52.2% for device D), which fully demonstrates the small efficiency roll-offs. The high efficiency and small roll-off could be ascribed to the highly efficient and balanced carrier transport abilities of **Az-NP-T** and **Az-NN-T**.

The operational lifetimes of devices A, B, C, and D were further evaluated in a constant current operation mode from an initial luminance of 25,000 cd m^{-2}, as shown in

TABLE 2 Electroluminescence characteristics of the top-emitting devices.

Devices	Host	λ_{EL} [nm]	V_{on} [a)] [V]	EQE [b)/c)/d)/e)] [%]	CE_{max} [cd A^{-1}]	PE_{max} [lm W^{-1}]	LT_{95}@L_1 [f)/g)/h)] [hours]	CIE [*x*,*y*]
A	**Az-P-T**	626	2.9	54.2/53.0/50.2/44.4	62.1	60.7	54/772/12850	(0.69,0.31)
B	**Az-TP-T**	626	3.4	46.2/46.2/45.3/41.5	57.4	50.8	18/257/4283	(0.69,0.31)
C	**Az-NP-T**	628	2.7	57.3/54.1/50.7/44.6	62.5	65.6	117/1673/27841	(0.69,0.31)
D	**Az-NN-T**	628	2.8	55.0/54.1/52.2/46.9	61.2	64.6	126/1802/29983	(0.69,0.31)

[a)]Turn-on voltages.
[b)/c)/d)/e)]EQE_{max}, EQE at 5000, 10,000, and 25,000 cd m^{-2}.
[f)/g)/h)]LT_{95} at 25,000, 5000, 1000 cd m^{-2}.

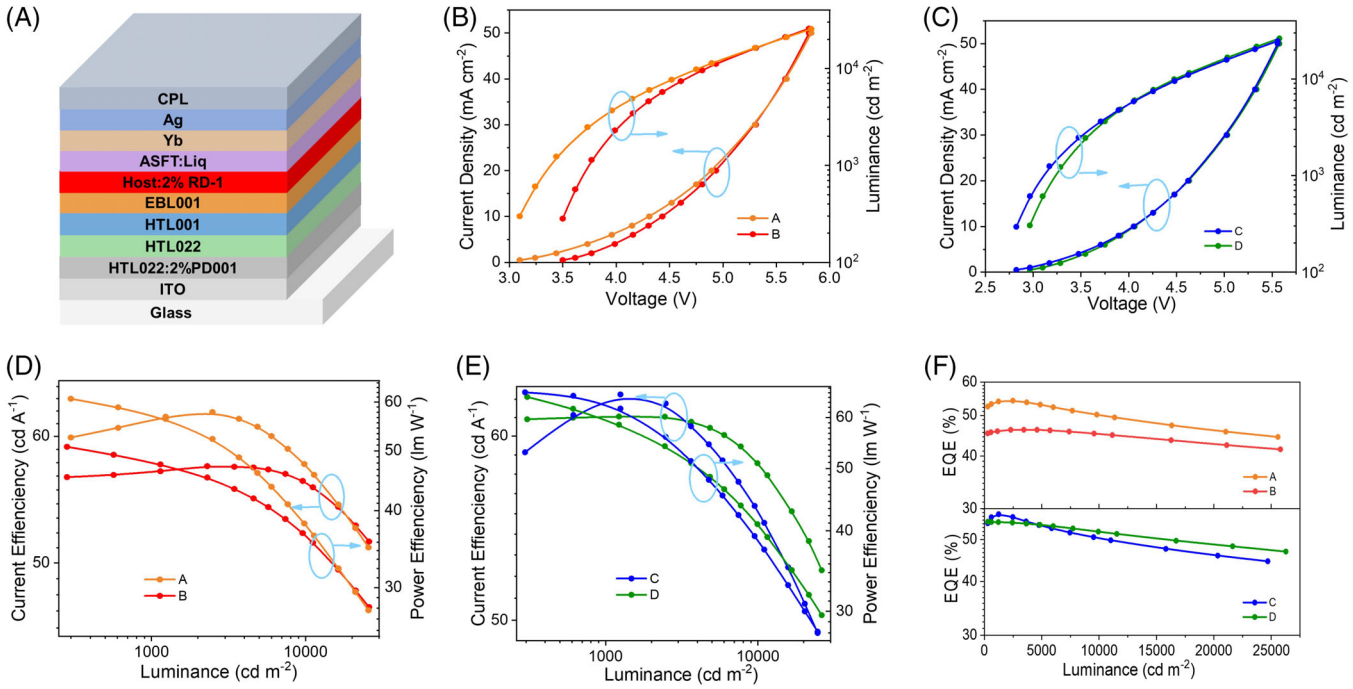

FIGURE 5 (A) Top-emitting device architecture. (B) and (C) Current density–voltage–luminance (*J*–*V*–*L*) curves. (D) and (E) Current efficiency–luminance–power efficiency (CE–L–PE) characteristics. (F) EQE–luminance curve for devices A, B, C, and D.

Figure 6. At 50 mA cm^{-2}, the devices demonstrated the time required for decreasing the luminance from the initial luminance to 95% of initial luminance (LT_{95}), which is 54, 18, 117, and 126 h, respectively. According to the formula $LT(L_1) = LT(L_0)(L_0/L_1)^n$ the lifetime at an initial luminance of 5000 and 1000 cd m^{-2} can be estimated, as shown in Table 2, where L_1 is the desired luminance and the exponent *n* here is using $n = 1.7$.[21] The results demonstrated that devices C and D based on **Az-NP-T** and **Az-NN-T** possess LT_{95} = 27,841 and 29,983 h (initial luminance of 1000 cd m^{-2}), respectively, which is much longer than that of devices A (LT_{95} = 12,850 h) and B (LT_{95} = 4,283 h). The high performance and stability of devices C and D could also be ascribed to the highly efficient and balanced carrier transport abilities of the **Az-NP-T** and **Az-NN-T** host.

3 | CONCLUSION

In summary, four ortho-substituted TADF molecules, **Az-P-T**, **Az-TP-T**, **Az-NP-T**, and **Az-NN-T**, with different linking groups, were synthesized and characterized. These four molecules show TADF emissions and fast RISC processes due to their twisted molecular configurations and short spatial distance between the aza-azulene donor and triazine plane. Moreover, **Az-NP-T** and **Az-NN-T** exhibit balanced hole and electron transport ability thanks to their larger acceptor stacking induced by the twisted naphthalene linker. Compared with the planar linking units, twisted linkers cannot stack well with the planar triazine unit of another molecules, while this can promote the formation of better π-stacking between its triazine group and the adjacent triazine group, resulting in an additional channel for electron transport. We may be the first to notice this unexpected phenomenon and offer a plausible explanation. Using these molecules as hosts, highly efficient and stable deep-red OLED with the EQE of 57.3% (device C), 55.0% (device D), and long device lifetime LT_{95} (initial luminance of 1000 cd m^{-2}) of 27,841 (device C) and 29,983 h (device D) were accessed. It turned out that for the matrix of phosphorescent OLEDs, the efficient transfer of charge and energy was a lot more critical than its own PLQY. Further research may reveal more about the structure–performance relationship of molecules and how to improve their charge and energy transfer in organic electronics.

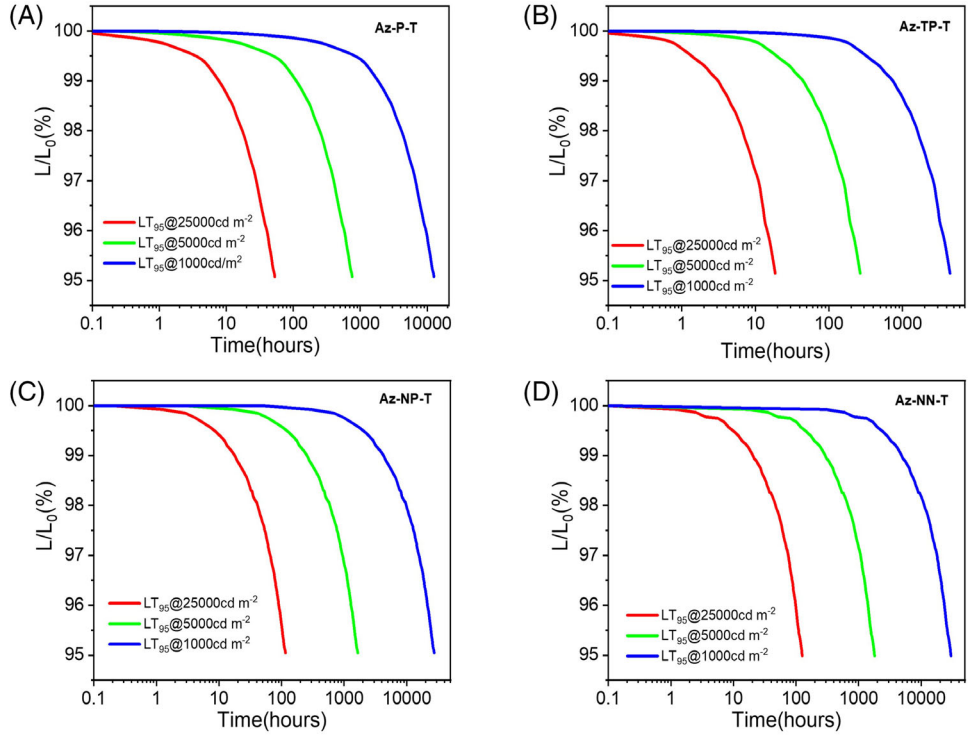

FIGURE 6 The operational lifetimes of devices A, B, C, and D are 25,000, 5000, and 1000 cd m^{-2}, respectively.

ACKNOWLEDGMENTS

This work was financially supported by the National Key R&D Program of China (No. 2022YFE0109000), the National Natural Science Foundation of China (No. 21975152), the China Postdoctoral Science Foundation (No. 2022M722028), and the Deutsche Forschungsgemeinschaft (DFG) under Germany's Excellence Strategy−3DMM2O−EXC−2082/1−390761711. We thank HZWTECH for providing computation facilities and Shuoqi Sun for discussions regarding this study.

Open access funding enabled and organized by Projekt DEAL.

CONFLICT OF INTEREST STATEMENT

The authors declare no conflicts of interest.

DATA AVAILABILITY STATEMENT

The data that support the findings of this study are available from the corresponding author upon reasonable request.

ORCID

Zixing Wang https://orcid.org/0000-0002-0814-8822

REFERENCES

1. a) H. Uoyama, K. Goushi, K. Shizu, H. Nomura, C. Adachi, *Nature* **2012**, *492*, 234. b) X.-C. Fan, K. Wang, Y.-Z. Shi, Y.-C. Cheng, Y.-T. Lee, J. Yu, X.-K. Chen, C. Adachi, X.-H. Zhang, *Nat. Photonics* **2023**, *17*, 280. c) G. Hong, X. Gan, C. Leonhardt, Z. Zhang, J. Seibert, J. M. Busch, S. Bräse, *Adv. Mater.* **2021**, *33*, 2005630. d) Y. Im, M. Kim, Y. J. Cho, J.-A Seo, K. S. Yook, J. Y. Lee, *Chem. Mater.* **2017**, *29*, 1946. e) H. Jiang, P. Tao, W.-Y. Wong, *ACS Materials Lett.* **2023**, *5*, 822.
2. a) Z. Qiu, W. Xie, Z. Yang, J.-H. Tan, Z. Yuan, L. Xing, S. Ji, W.-C. Chen, Y. Huo, S.-J. Su, *Chem. Eng. J.* **2021**, *415*, 128949. b) X. Zhang, J.-Y. Li, K. Zhang, L. Ding, C.-K. Wang, M.-K. Fung, J. Fan, *J. Mater. Chem. C* **2022**, *10*, 3685. c) D. T. Yonemoto, C. M. Papa, C. Mongin, F. N. Castellano, *J. Am. Chem. Soc.* **2020**, *142*, 10883. d) A. J. Gillett, R. H. Friend, D. Beljonne, *Chem. Mater.* **2022**, *34*, 7095.
3. a) X. Lv, Y. Wang, N. Li, X. Cao, G. Xie, H. Huang, C. Zhong, L. Wang, C. Yang, *Chem. Eng. J.* **2020**, *402*, 126173. b) Z. Yang, X. Ge, W. Li, Z. Mao, X. Chen, C. Xu, F. Long Gu, Y. Zhang, J. Zhao, Z. Chi, *Chem. Eng. J.* **2022**, *442*, 136219. c) J.-R. Cha, C. W. Lee, J. Y. Lee, M.-S. Gong, *Dyes Pigm.* **2016**, *134*, 562.
4. A. Endo, K. Sato, K. Yoshimura, T. Kai, A. Kawada, H. Miyazaki, C. Adachi, *Appl. Phys. Lett.* **2011**, *98*, 083302.
5. a) D. R. Lee, J. M. Choi, C. W. Lee, J. Y. Lee, *ACS Appl. Mater. Interfaces* **2016**, *8*, 23190. b) D. R. Lee, B. S. Kim, C. W. Lee, Y. Im, K. S. Yook, S. H. Hwang, J. Y. Lee, *ACS Appl. Mater. Interfaces* **2015**, *7*, 9625.
6. X. K. Chen, Y. Tsuchiya, Y. Ishikawa, C. Zhong, C. Adachi, J. L. Bredas, *Adv. Mater.* **2017**, *29*, 1702767.
7. a) H. van Eersel, P. A. Bobbert, R. A. J. Janssen, R. Coehoorn, *Appl. Phys. Lett.* **2014**, *105*, 143303. b) C. Murawski, K. Leo, M. C. Gather, *Adv. Mater.* **2013**, *25*, 6801.
8. a) C.-Y. Chan, M. Tanaka, Y.-T. Lee, Y.-W. Wong, H. Nakanotani, T. Hatakeyama, C. Adachi, *Nat. Photonics* **2021**, *15*, 203. b) N. C. Giebink, S. R. Forrest, *Phys. Rev. B* **2008**, *77*, 235215.
9. a) D. Zhang, M. Cai, Y. Zhang, D. Zhang, L. Duan, *Mater. Horiz.* **2016**, *3*, 145. b) D. R. Lee, S. H. Hwang, S. K. Jeon, C. W. Lee, J. Y. Lee, *Chem. Commun.* **2015**, *51*, 8105. c) P. L. Dos Santos, J. S. Ward, M. R. Bryce, A. P. Monkman, *J. Phys. Chem. Lett.* **2016**, *7*, 3341.
10. a) S. W. Li, C. H. Yu, C. L. Ko, T. Chatterjee, W. Y. Hung, K. T. Wong, *ACS Appl. Mater. Interfaces* **2018**, *10*, 12930. b) M. Godumala, S. Choi, S. K. Kim, S. W. Kim, J. H. Kwon, M. J. Cho, D. H. Choi, *J. Mater. Chem. C* **2018**, *6*, 10000. c) J. Chen, C. Shi, Q. Fu, F. Zhao, Y. Hu, Y. Feng, D. Ma, *J. Mater. Chem.* **2012**, *22*, 5164. d) Y. K. Wang, S. H. Li, S. F. Wu, C. C. Huang, S. Kumar, Z. Q. Jiang, M. K. Fung, L. S. Liao, *Adv. Funct. Mater.* **2018**, *28*, 1706228.
11. a) A. Kumar, W. Lee, T. Lee, J. Jung, S. Yoo, M. H. Lee, *J. Mater. Chem. C* **2020**, *8*, 4253. b) Y. C. Cheng, X. C. Fan, F. Huang, X. Xiong, J. Yu, K. Wang, C. S. Lee, X. H. Zhang, *Angew. Chem. Int. Ed.* **2022**, *61*, e202212575. c) J. X. Chen, W. W. Tao, Y. F. Xiao, K. Wang, M. Zhang, X. C. Fan, W. C. Chen, J. Yu, S. Li, F. X. Geng, X. H. Zhang, C. S. Lee, *ACS Appl. Mater. Interfaces* **2019**, *11*, 29086. d) H. Kang, S. G. Ihn, I. Kim, Y. S. Chung, S. O. Jeon, M. Sim, J. Kim, H. Lee, Y. Son, W. J. Son, I. Jang, D. S. Kim, H. Choi, J. P. Hong, *Adv. Opt. Mater.* **2022**, *10*, 2102309.

12. a) T. Zhang, M. Zhu, J. Li, Y. Zhang, X. Wang, *Dyes Pigm*. **2021**, *192*, 109426. b) D. R. Lee, C. W. Lee, J. Y. Lee, *J. Mater. Chem. C* **2014**, *2*, 7256. c) Y. Tao, Q. Wang, C. Yang, Q. Wang, Z. Zhang, T. Zou, J. Qin, D. Ma, *Angew. Chem. Int. Ed.* **2008**, *47*, 8104. d) X. K. Liu, C. J. Zheng, J. Xiao, J. Ye, C. L. Liu, S. D. Wang, W. M. Zhao, X. H. Zhang, *Phys. Chem. Chem. Phys.* **2012**, *14*, 14255. e) D. Wagner, S. T. Hoffmann, U. Heinemeyer, I. Münster, A. Köhler, P. Strohriegl, *Chem. Mater.* **2013**, *25*, 3758.
13. a) X. Lv, Y. Wang, N. Li, X. Cao, G. Xie, H. Huang, C. Zhong, L. Wang, C. Yang, *Chem. Eng. J.* **2020**, *402*, 12609. b) R. R. Xia, Z. Zhang, P. Wu, Y. J. Wu, K. Wang, X. F. Li, M. L. Ye, Z. X. Wang, *Chem. Eng. J.* **2024**, *479*, 147562.
14. Z. Wang, H. Shao, J. Ye, L. Zhang, P. Lu, *Adv. Funct. Mater.* **2007**, *17*, 253.
15. a) J. Luo, Z. Xie, J. W. Y. Lam, L. Cheng, H. Chen, C. Qiu, H. S. Kwok, X. Zhan, Y. Liu, D. Zhu, B. Z. Tang. *Chem. Commun.* **2001**, 1740. b) Y. Hong, J. W. Y. Lam, B. Z. Tang. *Chem. Soc. Rev.* **2011**, *40*, 5361. c) G. Yang, Y. Ran, Y. Wu, M. Chen, Z. Bin, J. You, *Aggregate* **2022**, *3*, e127. d) H. Wu, X.-C. Fan, H. Wang, F. Huang, X. Xiong, Y.-Z. Shi, K. Wang, J. Yu, X.-H. Zhang, *Aggregate* **2023**, *4*, e243. e) J. Hwang, P. Nagaraju, M. J. Cho, D. H. Choi, *Aggregate* **2023**, *4*, e199.
16. a) Z. Wang, Z. Li, Y. Zhang, W. Liu, *J. Chem. Phys.* **2020**, *153*, 164109. b) Z. Li, Y. Xiao, W. Liu, *J. Chem. Phys.* **2014**, *141*, 054111. c) W. Liu, F. Wang, L. Li, *J. Theor. Comput. Chem.* **2003**, *02*, 257.
17. a) Z. Liu, T. Lu, Q. Chen, *Carbon* **2020**, *165*, 461. b) T. Lu, F. Chen, *J. Comput. Chem.* **2012**, *33*, 580. c) T. Liang, X. Jiang, J. Wang, Y. Pan, B. Yang, *Comput. Theo. Chem.* **2023**, *1220*, 114000.
18. X. K. Chen, B. W. Bakr, M. Auffray, Y. Tsuchiya, C. D. Sherrill, C. Adachi, J. L. Bredas, *J. Phys. Chem. Lett.* **2019**, *10*, 3260.
19. a) Y. Wada, H. Nakagawa, S. Matsumoto, Y. Wakisaka, H. Kaji, *Nat. Photonics* **2020**, *14*, 643. b) L. Hua, Y. Liu, B. Liu, Z. Zhao, L. Zhang, S. Yan, Z. Ren, *Nat. Commun.* **2022**, *13*, 7828.
20. a) C. Deng, L. Zhang, D. Wang, T. Tsuboi, Q. Zhang, *Adv. Opt. Mater.* **2019**, *7*, 1801644. b) R. Skaisgiris, T. Serevičius, K. Kazlauskas, Y. Geng, C. Adachi, S. Juršėnas, *J. Mater. Chem. C* **2019**, *7*, 12601. c) Z. Zhang, D. H. Dou, R. R. Xia, P. Wu, E. Spuling, K. Wang, J. Cao, B. Wei, X. F. Li, J. H. Zhang, S. Bräse, Z. X. Wang, *Sci. Adv.* **2023**, *9*, eadf4060.
21. K. Masui, H. Nakanotani, C. Adachi, *Org. Electron.* **2013**, *14*, 2721.
22. a) M. Baba, *J. Phys. Chem. A* **2011**, *115*, 9514. b) F. B. Dias, J. Santos, D. R. Graves, P. Data, R. S. Nobuyasu, M. A. Fox, A. S. Batsanov, T. Palmeira, M. N. Berberan-Santos, M. R. Bryce, A. P. Monkman, *Adv. Sci.* **2016**, *3*, 1600080.
23. a) I. S. Park, K. Matsuo, N. Aizawa, T. Yasuda, *Adv. Funct. Mater.* **2018**, *28*, 1802031. b) P. K. Samanta, D. Kim, V. Coropceanu, J. L. Bredas, *J. Am. Chem. Soc.* **2017**, *139*, 4042.
24. T. Fleetham, G. Li, J. Li, *ACS Appl. Mater. Interfaces* **2015**, *7*, 16240.

SUPPORTING INFORMATION

Additional supporting information can be found online in the Supporting Information section at the end of this article.

How to cite this article: Z. Zhang, R. Xia, K. Wang, Y. Wu, P. Zang, X. Gan, Z. Liao, B. Wei, P. Wu, S. Bräse, Z. Wang, *Aggregate* **2024**, e588. https://doi.org/10.1002/agt2.588